A&A 541, A71 (2012)
DOI: 10.1051/0004-6361/201218823

Astronomy & Astrophysics

The dusty environment of HD 97300 as seen by *Herschel* and *Spitzer*⋆

Á. Kóspál[1], T. Prusti[1], N. L. J. Cox[2], G. L. Pilbratt[1], Ph. André[3], C. Alves de Oliveira[4], E. Winston[1], B. Merín[4], A. Ribas[4], P. Royer[2], R. Vavrek[4], and C. Waelkens[2]

[1] Research and Scientific Support Department, European Space Agency (ESA-ESTEC, SRE-SA), PO Box 299, 2200 AG Noordwijk, The Netherlands
e-mail: akospal@rssd.esa.int
[2] Instituut voor Sterrenkunde, KU Leuven, Celestijnenlaan 200D, 3001 Leuven, Belgium
[3] Laboratoire AIM Paris – Saclay, CEA/DSM – CNRS – Université Paris Diderot, IRFU, Service d'Astrophysique, Centre d'Études de Saclay, Orme des Merisiers, 91191 Gif-sur-Yvette, France
[4] Herschel Science Centre, ESA-ESAC, PO Box 78, 28691 Villanueva de la Cañada, Madrid, Spain

Received 15 January 2012 / Accepted 2 March 2012

ABSTRACT

Aims. We analyze the surroundings of HD 97300, one of two intermediate-mass stars in the Chamaeleon I star-forming region. The star is known to be surrounded by a conspicuous ring of polycyclic aromatic hydrocarbons (PAHs).
Methods. We present infrared images taken with *Herschel* and *Spitzer* using 11 different broad-band filters between 3.6 μm and 500 μm. We compare the morphology of the emission using cuts along different position angles. We construct spectral energy distributions, which we compare to different dust models, and calculate dust temperatures. We also derive opacity maps and analyze the density structure of the environment of HD 97300.
Results. We find that HD 97300 has no infrared excess at or below 24 μm, confirming its zero-age main-sequence nature. The morphology of the ring is very similar between 3.6 μm and 24 μm. The emission at these wavelengths is dominated by either PAH features or PAH continuum. At longer wavelengths, only the northwestern part of the ring is visible. A fit to the 100–500 μm observations suggests that the emission is due to relatively warm (≈26 K) dust. The temperature gradually decreases with increasing distance from the ring. We find a general decrease in the density from north to south, and an approximate 10% density increase in the northeastern part of the ring.
Conclusions. Our results are consistent with the theory that the ring around HD 97300 is essentially a bubble blown into the surrounding interstellar matter and heated by the star.

Key words. circumstellar matter – stars: formation – stars: individual: HD 97300 – stars: pre-main sequence – infrared: ISM – ISM: lines and bands

1. Introduction

At a distance of 160 pc, Chamaeleon I is one of the closest and richest star-forming regions, containing about 200 known low-mass young stellar objects (Whittet et al. 1997; Luhman et al. 2008). There are only two intermediate-mass stars in Chamaeleon I: HD 97048 in the southern part of the cloud and HD 97300 in the northern part. While HD 97048 is a bona fide Herbig Ae/Be star, HD 97300 seems to be older, and is probably a zero-age main-sequence star (e.g. Assendorp et al. 1990, and references therein). Excess emission with respect to a B9-type stellar photosphere was detected at infrared wavelengths towards HD 97300, and was first attributed to an M-type companion or a circumstellar dust shell (Hyland et al. 1982; Wesselius et al. 1984; Thé et al. 1986). On the basis of maps of both optical extinction and 130 μm optical depth, Jones et al. (1985) found that HD 97300 sits in the middle of a low-density region. They interpreted this result in terms of a bubble cleared out by the (now ended) stellar wind of HD 97300.

Prusti et al. (1994) later discovered that the 8–13 μm emission is extended, while Siebenmorgen et al. (1998) were able to resolve the source with the Infrared Space Observatory at mid-infrared wavelengths, finding that HD 97300 is surrounded by an elliptical ring of size about 50″ × 36″. The emission of the ring is dominated by emission bands from polycyclic aromatic hydrocarbons (PAHs) at 6.2, 7.7, 8.7, 11.3, and 12.5 μm (for a general review of PAHs, see e.g. Tielens 2008). Siebenmorgen et al. (1998) modeled the ring with a mixture of PAHs, very small grains, and large grains, and speculated that the ring consists of interstellar matter entrained by either mass loss or radiation pressure from the B9-type star. Using optical polarization measurements, Andersson & Potter (2010) found evidence of a local enhancement in the dust heating and radiatively driven grain alignment.

In this paper, we present a comprehensive analysis of the surroundings of HD 97300 using infrared images covering a large wavelength range from 3.6 μm to 500 μm. In Sect. 2, we briefly describe the reduction of the images taken with the *Herschel*

⋆ This work is based on observations made with the *Herschel* Space Observatory and with the *Spitzer* Space Telescope. *Herschel* is an ESA space observatory with science instruments provided by European-led Principal Investigator consortia and with important participation from NASA. *Spitzer* is operated by the Jet Propulsion Laboratory, California Institute of Technology under a contract with NASA.

Space Observatory (Pilbratt et al. 2010) and the *Spitzer* Space Telescope (Werner et al. 2004). In Sect. 3, we present images and brightness profiles along different position angles. In Sect. 4, we discuss the multiplicity of HD 97300, and we analyze the spectral energy distribution (SED) of the ring to constrain different dust models. In Sect. 5, we summarize our conclusions.

2. Observations

HD 97300 was observed with *Herschel* in January 2011 as part of the "Herschel Gould Belt survey" (André et al. 2010), using the PACS (Poglitsch et al. 2010) and the SPIRE (Griffin et al. 2010) instruments. Images at 70, 160, 250, 350, and 500 μm images were obtained simultaneously in SPIRE/PACS parallel mode. Additional PACS-only 100 and 160 μm images were also taken. Details of the data reduction are described in papers by Winston et al. (2012) and Vavrek et al. (in prep.).

HD 97300 was also observed with *Spitzer* in July 2004. IRAC images at 3.6, 4.5, 5.8, and 8.0 μm were taken in High Dynamic Range mode, alternating between exposure times of 10.4 s and 0.4 s (aor 3651328). We downloaded the saturation-corrected basic calibrated data (CBCD) produced by the pipeline version S18.18.0 at the *Spitzer* Science Center. We used MOPEX (Makovoz et al. 2006) to create a mosaic from the individual frames. Several pixels around HD 97300 were saturated in the long exposure mosaic. To ensure that we acquired data of good signal-to-noise ratio for the faint extended emission, but also correct fluxes for the bright point sources, we created a final image by taking the long exposure image and replacing the pixels affected by saturation with the corresponding pixels from the short exposure image. Pixels unaffected by saturation had identical flux values in the long and short exposure images within the measurement uncertainties. MOPEX was also used to create mosaics from the MIPS 24 μm and 70 μm images (aor 3661312). At 24 μm, we used the basic calibrated data (BCD), while at 70 μm, we used the median-subtracted, time-filtered FBCD files. Exposure times for MIPS were 3.67 s at 24 μm and 4.19 s at 70 μm, and on average 20 frames at 24 μm and 10 frames at 70 μm were used to create the final mosaics. Saturation was not an issue at these wavelengths.

3. Results

Figure 1 presents $2' \times 2'$ images centered on HD 97300 at 11 different infrared wavelengths. We do not show the MIPS 70 μm image, because after convolving the higher spatial resolution PACS 70 μm image to match the resolution of the MIPS 70 μm image (using the convolution kernels of Gordon et al. 2008), we found that they agree to within 20%. At 160 μm, we show merely the PACS-only mode image in Fig. 1, because it is essentially identical to the SPIRE/PACS parallel mode 160 μm image. Our 3.6–24 μm images clearly show the same narrow elliptical ring around HD 97300 imaged by Siebenmorgen et al. (1998) at 6.0–14.9 μm. A point source coinciding with HD 97300 is seen between 3.6 μm and 8.0 μm, but a second peak also appears at 8.0 μm about 3–4″ north of HD 97300. This peak was previously detected by Siebenmorgen et al. (1998) at 11.3 μm and 14.9 μm. The strength of HD 97300 relative to the ring gradually decreases with increasing wavelength and the star is indeed invisible at 24 μm and above. While the ring is relatively symmetric (its northeastern part being similar to its southwestern part) at shorter wavelengths, its northeastern part is much more prominent at 70 μm, an effect that is even more pronounced at 100 and 160 μm. A bright patch of emission to the north of HD 97300, probably originating in the Chamaeleon I cloud, starts appearing at 100 μm. At the SPIRE wavelengths, this patch dominates the images, although emission from the northeastern part of the ring remains visible.

To quantitatively analyze the images, in Fig. 2 we plotted the brightness profiles at different wavelengths along two perpendicular lines across the star, one at a PA of 142° (NW–SE), the other one at 52° (SW–NE), as indicated by the lines in the upper right panel of Fig. 1. For comparison, we also plotted the observed point spread functions (PSFs), which were constructed by taking the median of the normalized images of four-to-six isolated stars in the field, then taking cuts along the same PAs as mentioned before. Following Siebenmorgen et al. (1998), we scaled the observed PSFs to ensure that at each wavelength they correspond to the expected flux of a black body with a temperature of 10 700 K. Figure 2 shows that while at 3.6, 4.5, and 5.8 μm the star dominates the observed flux (being at least an order of magnitude brighter than the surrounding diffuse emission), the star and the ring contribute almost comparably at 8.0 μm, and the stellar contribution is essentially negligible at 24 μm and above. Given that the observed profiles are consistent with HD 97300 having a photospheric flux at 8 μm and below, we can derive the following stellar fluxes: $F_{3.6} = 0.41$ Jy, $F_{4.5} = 0.28$ Jy, $F_{5.8} = 0.17$ Jy, and $F_{8.0} = 0.09$ Jy. The uncertainty in these numbers is about 15%. The error is dominated by the difficulty in determining the precise background. From the non-detection of HD 97400 at longer wavelengths, we can infer upper limits to the stellar fluxes of $F_{24} < 0.012$ Jy and $F_{70} < 0.06$ Jy (cf. the expected photospheric fluxes of 0.011 Jy at 24 μm and 0.001 Jy at 70 μm). This result is consistent with the star having no measurable infrared excess at or below 24 μm. The SED of the star is plotted with gray dots in the upper panel of Fig. 3.

Apart from the point source, extended emission is clearly seen in the IRAC cuts plotted in Fig. 2. Starting from the northwest, we see gradually increasing fluxes up to the point where the star is situated. A steep decline follows, then there is another peak, corresponding to the part of the ring farthest from the star. As indicated by the dashed line in Fig. 2, this peak is always located at a distance of 20″ from the star, irrespective of the wavelength. Although the exact wavelengths are different, the shape of our NW-SE cuts are in general consistent with the cuts plotted in Fig. 4 of Siebenmorgen et al. (1998) and we see no signs of the expansion of the ring.

4. Discussion

4.1. Multiplicity of HD 97300

HD 97300 is a subarcsecond binary with a separation of 0.″8, PA of 327°, and near-infrared magnitude differences of $\Delta H = 3.33$ mag, $\Delta K = 3.05$ mag (Ghez et al. 1997; Lafrenière et al. 2008). We do not resolve the binary system at any infrared wavelength. Considering the near-infrared brightness ratios and that the companion is probably a low-mass star, the contribution of the companion to the photometry of HD 97300 should be at most 5–10%. Siebenmorgen et al. (1998) detected a second peak about 3–4″ north of HD 97300 at 11.3 μm and 14.9 μm, although not at shorter wavelengths, and speculated that it may be an embedded companion. We also detected this peak at 8.0 μm, but at our spatial resolution, it is clearly resolved and not point-like (see also the lower panel of Fig. 2, where the secondary peak is visible on the IRAC 8.0 μm cut at the position of about 4–5″). The lack of any source detected at this position in the 870 μm

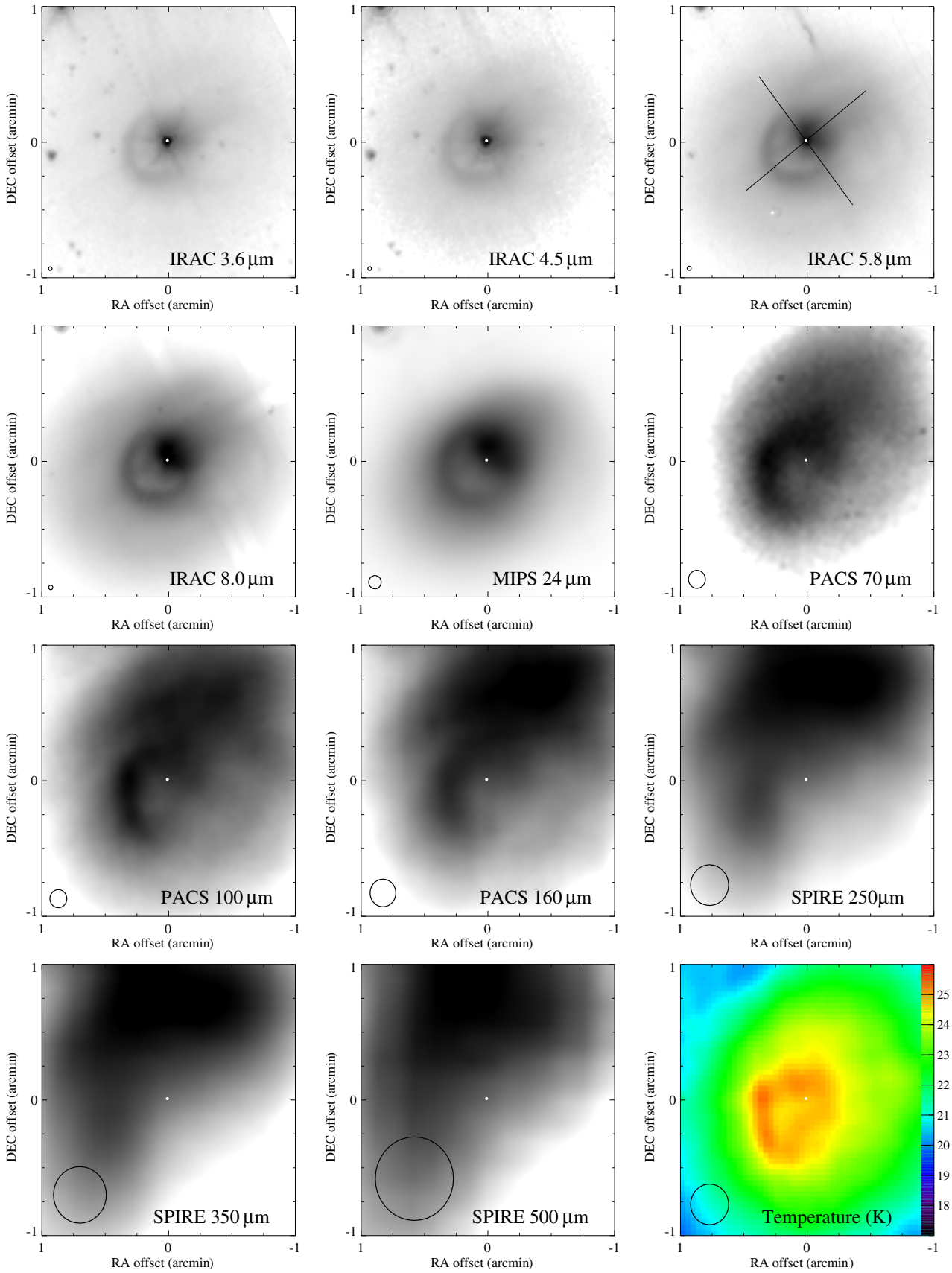

Fig. 1. Images of HD 97300 at different wavelengths. The coordinates are relative to $RA_{2000} = 11^h09^m50\overset{s}{.}02$ $Dec_{2000} = -76°36'47\overset{''}{.}72$. The scaling is logarithmic. Each panel is $2' \times 2'$, and north is up, east is left. The diameter of the circles in the bottom left corners corresponds to the FWHM of the PSF. The small white dot in each image indicates the stellar position. The lines in the *upper right panel* show the directions along which the cuts in Fig. 2 were measured. The *bottom right panel* shows the dust temperature on a linear scale as measured by fitting a modified black body to the 100, 160, and 250 μm images (see the text for details).

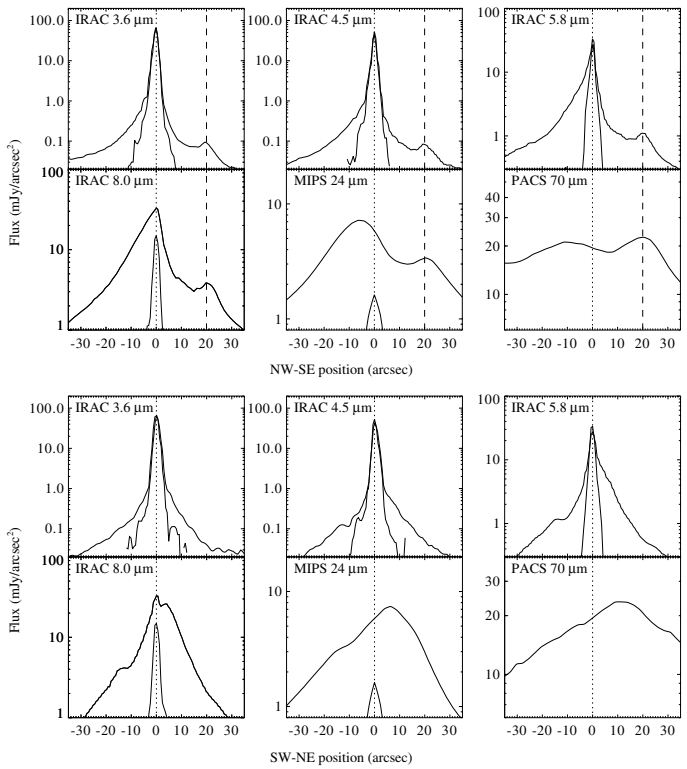

Fig. 2. Logarithmic brightness profiles. The NW-SE cut was measured along a PA of 142°, the SW-NE cut along a PA of 52°. These directions are marked with lines in the upper right panel of Fig. 1. The vertical dotted line indicates the stellar position, while the vertical dashed line indicates the ring. The thin lines show the PSF scaled to the expected stellar brightness (for more details, see the text).

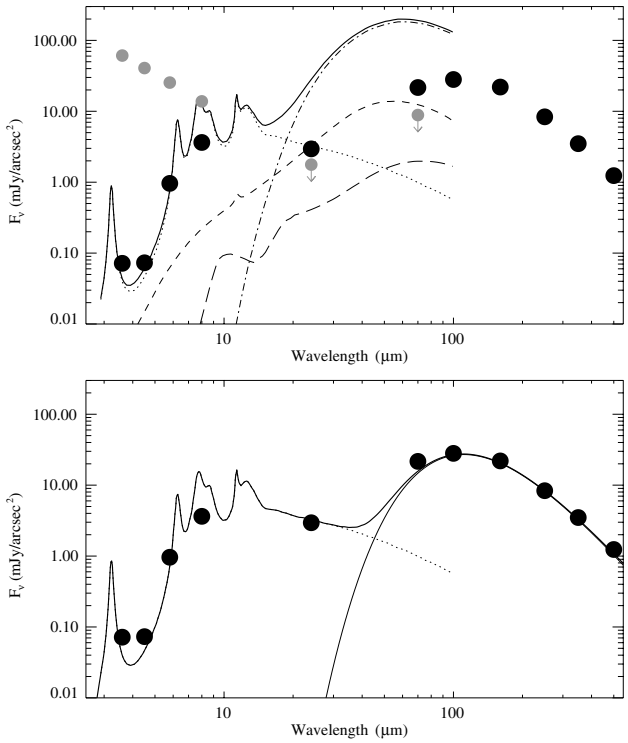

Fig. 3. *Upper panel*: dust model for the ring from Siebenmorgen et al. (1998). Dotted line: PAHs; dashed line: very small graphite; long dashed line: very small silicates; dash-dotted line: large grains. The small gray dots (from this work) mark the observational data or upper limits for the stellar photosphere, while the large black dots (also from this work) represent the ring emission as measured at a distance of 20″, PA of 142° from the star (position 7 in Siebenmorgen et al. 1998). Error bars are smaller than the symbol sizes, thus they are not plotted. *Lower panel*: the large black dots are the same observations as in the upper panel, but the overplotted model (thick solid line) is the sum of the PAHs from Siebenmorgen et al. (1998) (dotted line) and a single-temperature modified black body (thin solid line) with $T = 26.0$ K and $\beta = 2.0$.

continuum map of Belloche et al. (2011) also argues against the embedded companion scenario. Although we cannot completely exclude the possibility that a core is associated with HD 97300, the extended nature of the peak and that it is only seen at 8.0, 11.3, and 14.9 μm, strongly suggest that it is related to PAHs. It may be a localized enhancement in PAHs, or an area where the excitation conditions are more favorable.

4.2. PAH emission

Using spectrally resolved mid-infrared images, Siebenmorgen et al. (1998) performed a detailed analysis of the ring around HD 97300. They fitted the observed spectra with a mixture of PAHs, very small particles, and large grains (Fig. 3, upper panel). They found that below 16 μm, the emission is dominated by PAH features. Very small graphite and silicate grains have at least a one order of magnitude smaller contribution at all wavelengths. Above about 16 μm, the model is dominated by the thermal emission of large grains, although continuum emission from PAHs is also included in their model. However, in the absence of longer wavelength data, they were unable to check the validity of the model at wavelengths longer than 16 μm.

In the upper panel of Fig. 3, we reproduced Fig. 3 from Siebenmorgen et al. (1998). We also overplotted the observed brightness of the ring in our *Spitzer* and *Herschel* images at a distance of 20″, for the PA of 142° of the star, corresponding to the position for which the dust model in Fig. 3 was calculated in Siebenmorgen et al. (1998). There is good agreement between the observed brightness and the model for the four IRAC filters, but there is a large discrepancy between the observations and the model at longer wavelengths, where Siebenmorgen et al. (1998) had no information about the brightness of the ring. The IRAC 4.5 μm filter mostly samples a pseudo-continuum between the 3.3 μm and 6.2 μm PAH features. The other three IRAC filters cover strong PAH features. In agreement with the model, the extended emission in Fig. 2 indeed appears to be at its brightest in the 8 μm image, which includes the strong 7.7 μm feature.

Judging from the dust model, the 24, 70, and 100 μm images should be the most well-suited to study the large grain population. On the basis of the distance of the ring from the central star, Siebenmorgen et al. (1998) estimated a temperature of 50 K and predicted that the emission would peak at about 60 μm. Our observations, however, suggest that the peak is instead somewhere between 70 μm and 160 μm, indicating that there is no warm (50 K) dust in the system. The observed 24 μm brightness can still be fully explained by PAHs. The morphology of the ring between 3.6 μm and 24 μm remains almost unchanged, supporting the idea that the emission in this wavelength range is coming almost exclusively from PAH molecules.

4.3. Warm dust

At 70 μm and above, PAH emission can no longer explain the observed SED of the ring. The upper panel of Fig. 3 shows that

we need colder (<50 K) dust to fit the observations. If we take into account data points from 100 μm to 500 μm, the SED can be well-fitted with a modified black body (Fig. 3, lower panel). The best-fit model has a temperature of $T = 26.0$ K for a fixed power-law index of the dust opacity coefficient $\beta = 2.0$ (assuming a dust opacity law of $\kappa \propto \lambda^{-\beta}$). For the diffuse interstellar medium, $\beta \approx 1.8$ (Draine 2006), while grain growth results in $\beta \lesssim 1$ (Beckwith & Sargent 1991). That a black body with $\beta = 2$ fits the observed data points very well suggests that the ring around HD 97300 contains interstellar medium-like dust. Interestingly, the ratio of the total to selective extinction, $R_V = A_V/E(B-V)$ for HD 97300 is around 4.9–5.5 (Grasdalen et al. 1975; Steenman & Thé 1989a). For the diffuse interstellar medium, the typical value of R_V is 3.1, while grain growth leads to larger R_V values (Steenman & Thé 1989b; Cardelli et al. 1989). This is not necessarily a contradiction for the following reason. The value of R_V is very sensitive to small variations in the grain size. A change of the maximal grain size from 0.22 μm to 1 μm results in an increase of R_V from 3.1 to 5.9 (see Fig. 3 in Steenman & Thé 1989b). The value of β derived from the slope of the sub-millimeter SED, on the other hand, only changes significantly if the grains grow to several tens of microns (see Fig. 3 in Draine 2006). Thus, some grain growth has occurred in the vicinity of HD 97300, but the grains remain no larger than a micrometer size. We note that another solution to the difficulty in reconciling the observed R_V and β may be that they trace different parcels of dust. While optical and near-infrared data (yielding R_V) probe only line-of-sight material in front of the star, far-infrared data (yielding β) might contain contributions from the dust in the underlying cloud.

Modified black-body fits could be obtained not only for the ring, but for any point in our data map of sufficiently high signal-to-noise ratio. We used the convolution kernels of Gordon et al. (2008) to smooth the 100 μm and 160 μm images to the resolution of the 250 μm image, and used these three images to fit modified black-body curves for each pixel with β fixed at 2.0. The resulting temperature map is plotted in the bottom right panel of Fig. 1. The ring around HD 97300 clearly stands out in the temperature map, with temperatures of around 25–26 K. The temperature gradually decreases with increasing distance from the ring to about 20–23 K. The morphology of the temperature map suggests that the dust in the ring around HD 97300 is heated by the central star, but not so much as the 50 K expected by Siebenmorgen et al. (1998). Interestingly, the dust temperature in the vicinity of HD 97300 is still higher than the typical temperatures in the Chamaeleon complex: Tóth et al. (2000) found that the intercloud material has a typical dust color temperature of ≈16.3 K, while the obscured clouds are ≤14.5 K. Ikeda et al. (2012) found two dust components in Chamaeleon I, a cold one with a temperature of 11.7 K, and a warm one with a temperature of 22.1 K. Thus, the immediate surroundings of HD 97300 are slightly warmer even than this warm component.

4.4. Density structure

Our results suggest that the long wavelength emission of the ring around HD 97300 originates in relatively warm (≈26 K) dust. Interestingly, practically the full ring is visible in the temperature map, while only the northeastern arc is clearly visible in 70–250 μm emission. This indicates that the dust density is probably higher in the northeastern part of the ring than in the southwestern part. To test this hypothesis, we derived opacity maps (τ_{100} and τ_{160}) using the temperature map and the 100 μm and 160 μm surface brightness maps plotted in Fig. 1. In terms of the large-scale structure, our opacity maps are remarkably similar to the τ_{130} map of Jones et al. (1985). The opacity is lower around HD 97300 and towards the south ($\tau_{100} \approx 0.8 \times 10^{-3}$), and higher farther from the star and to the north (up to $\tau_{100} \approx 1.8 \times 10^{-3}$ in the studied $2' \times 2'$ area). An important difference with respect to the opacity map of Jones et al. (1985) is that the high spatial resolution of our *Herschel* maps also enables us to study the density structure of the ring. Only the northeastern part of the ring is visible in our opacity maps, indicating that it is indeed denser than the southwestern part. The opacity (and thus density) contrast between the northeastern part of the ring and its surroundings is about 10%.

By averaging the opacity in a region within 33″ of the star, we get $\tau_{100} = 1 \times 10^{-3}$. Using $A_V/\tau_{100} = 1000$ mag as a typical value for the diffuse interstellar medium (Kiss et al. 2006), we can convert the far-infrared opacity to the optical extinction of $A_V = 1$ mag. Taking the relation between the optical extinction and the hydrogen column density from Güver & Özel (2009), we obtain $N_{\rm H} = 2.2 \times 10^{21}$ cm^{-2} (or 3.7×10^{-3} g cm^{-2}). This gives a total mass of 0.008 $M_\odot$ for this region. The mass in the ring is probably less than 10% of this value, that is about an order of magnitude less than the mass determined by Siebenmorgen et al. (1998) from their PAH observations (0.07 $M_\odot$ for the whole 33″-radius area, and 0.03 $M_\odot$ for the ring). Since these are order of magnitude calculations rather than precise modeling, these values are not inconsistent, but indicate the uncertainty in the estimates.

The temperature smoothly decreases farther from the ring, with no significant difference between the northern and southern sides. Thus, the bright patch of emission seen to the north of HD 97300 in the long wavelength maps in Fig. 1 probably also indicates a density enhancement to the north. The 870 μm continuum map of Belloche et al. (2011), as well as our opacity maps also suggest that there is a general increase in column density towards the north in the area of HD 97300. These findings support the theory that the ring around HD 97300 is essentially a bubble blown into the interstellar matter by the central star, either due to its stellar wind or its radiation pressure. The density (ρ) gradient of the interstellar dust in the vicinity of HD 97300 naturally explains the asymmetric and nonconcentric appearance of the ring, since the radius of a stellar wind bubble is proportional to $\rho^{-1.5}$ (Weaver et al. 1977).

5. Summary

We have presented infrared images of HD 97300 and its surroundings at 11 different wavelengths between 3.6 μm and 500 μm. By analyzing the brightness profiles across the star along different position angles, we have found that the star has no infrared excess at or below 24 μm, confirming its zero-age main-sequence nature. We constructed the SED of the ring based on our 11 data points and compared it to the dust model of Siebenmorgen et al. (1998). On the basis of the SED and the morphology of the emission at different wavelengths, we have concluded that our data set can be explained in terms of a two-component dust model. The emission up to 24 μm is consistent with that from PAH molecules, while at longer wavelengths, we observe thermal emission from relatively warm (≈26 K) dust. The emission above 70 μm suggests that there is an inhomogeneous distribution of the interstellar matter, and we conclude that the ring around HD 97300 is probably a bubble blown into the interstellar matter and heated by the star.

Acknowledgements. PACS has been developed by a consortium of institutes led by MPE (Germany) and including: UVIE (Austria); KUL, CSL, IMEC (Belgium); CEA, OAMP (France); MPIA (Germany); IFSI, OAP/AOT, OAA/CAISMI, LENS, SISSA (Italy); IAC (Spain). This development has been supported by the funding agencies BMVIT (Austria), ESA-PRODEX (Belgium), CEA/CNES (France), DLR (Germany), ASI (Italy), and CICT/MCT (Spain). SPIRE has been developed by a consortium of institutes led by Cardiff Univ. (UK) and including: Univ. Lethbridge (Canada); NAOC (China); CEA, LAM (France); IFSI, Univ. Padua (Italy); IAC (Spain); Stockholm Observatory (Sweden); Imperial College London, RAL, UCL-MSSL, UKATC, Univ. Sussex (UK); and Caltech, JPL, NHSC, Univ. Colorado (USA). This development has been supported by national funding agencies: CSA (Canada); NAOC (China); CEA, CNES, CNRS (France); ASI (Italy); MCINN (Spain); SNSB (Sweden); STFC (UK); and NASA (USA). P.R. and N.L.J.C. acknowledge support from the Belgian Federal Science Policy Office via the PRODEX Programme of ESA. The authors thank an anonymous referee, whose suggestions helped to improve this paper.

References

Andersson, B.-G., & Potter, S. B. 2010, ApJ, 720, 1045
André, P., Men'shchikov, A., Bontemps, S., et al. 2010, A&A, 518, L102
Assendorp, R., Wesselius, P. R., Prusti, T., & Whittet, D. C. B. 1990, MNRAS, 247, 624
Beckwith, S. V. W., & Sargent, A. I. 1991, ApJ, 381, 250
Belloche, A., Schuller, F., Parise, B., et al. 2011, A&A, 527, A145
Cardelli, J. A., Clayton, G. C., & Mathis, J. S. 1989, ApJ, 345, 245
Draine, B. T. 2006, ApJ, 636, 1114
Ghez, A. M., McCarthy, D. W., Patience, J. L., & Beck, T. L. 1997, ApJ, 481, 378
Gordon, K. D., Engelbracht, C. W., Rieke, G. H., et al. 2008, ApJ, 682, 336
Grasdalen, G., Joyce, R., Knacke, R. F., Strom, S. E., & Strom, K. M. 1975, AJ, 80, 117
Griffin, M. J., Abergel, A., Abreu, A., et al. 2010, A&A, 518, L3
Güver, T., & Özel, F. 2009, MNRAS, 400, 2050
Hyland, A. R., Jones, T. J., & Mitchell, R. M. 1982, MNRAS, 201, 1095
Ikeda, N., Kitamura, Y., Takita, S., et al. 2012, ApJ, 745, 48
Jones, T. J., Hyland, A. R., Harvey, P. M., Wilking, B. A., & Joy, M. 1985, AJ, 90, 1191
Kiss, C., Ábrahám, P., Laureijs, R. J., Moór, A., & Birkmann, S. M. 2006, MNRAS, 373, 1213
Lafrenière, D., Jayawardhana, R., Brandeker, A., Ahmic, M., & van Kerkwijk, M. H. 2008, ApJ, 683, 844
Luhman, K. L., Allen, L. E., Allen, P. R., et al. 2008, ApJ, 675, 1375
Makovoz, D., Roby, T., Khan, I., & Booth, H. 2006, in SPIE Conf. Ser., 6274
Pilbratt, G. L., Riedinger, J. R., Passvogel, T., et al. 2010, A&A, 518, L1
Poglitsch, A., Waelkens, C., Geis, N., et al. 2010, A&A, 518, L2
Prusti, T., Natta, A., & Palla, F. 1994, A&A, 292, 593
Siebenmorgen, R., Natta, A., Kruegel, E., & Prusti, T. 1998, A&A, 339, 134
Steenman, H., & Thé, P. S. 1989a, Ap&SS, 161, 99
Steenman, H., & Thé, P. S. 1989b, Ap&SS, 159, 189
Thé, P. S., Tjin A Djie, H. R. E., Steenman, H., & Wesselius, P. R. 1986, A&A, 155, 347
Tielens, A. G. G. M. 2008, ARA&A, 46, 289
Tóth, L. V., Hotzel, S., Krause, O., et al. 2000, A&A, 364, 769
Weaver, R., McCray, R., Castor, J., Shapiro, P., & Moore, R. 1977, ApJ, 218, 377
Werner, M. W., Roellig, T. L., Low, F. J., et al. 2004, ApJS, 154, 1
Wesselius, P. R., Beintema, D. A., & Olnon, F. M. 1984, ApJ, 278, L37
Whittet, D. C. B., Prusti, T., Franco, G. A. P., et al. 1997, A&A, 327, 1194
Winston, E., Prusti, T., Merín, B., et al. 2012, A&A, submitted